Forced Convection Heat Transfer and Flow in an Annular Porous Medium in the Non-Darcian Effects

السريان وانتقال الحراره بالحمل الجبرى خلال وسط مسامى حلقى مستدير تحت التأثيرات اللادارسيه

M. S. El Kady

Power Mechanical Engineering Department
El Mansoura University, Egypt

خلاصـــــه:

يبين هذا البحث دراسه عدديه للسريان وانتقال الحراره بالحمل الجبرى خلال مجرى حلقى مستدير مملوء بوسط مسامى درجات حراره الحوائط به ثابته. يتكون النموذج من معادله الطاقه بالاضافه الى معادله كميه الحركه بصورتها العامه والتى تشتمل على التأثيرات اللادارسيه المختلفه مثل المساميه المتغيره، التصور الذاتى للمائع والاحتكاك اللزج عند الحوائط، وقد استخدمت طريقه الفروق البسيطه فى الحل العددى. وللتأكد من صحه النتائج العدديه اجريت مقارنه مع النتائج التى حصل عليها بوليكاكوس ورينكن [6] أظهرت تطابقا جيدا واثبتت صحه هذا النموذج. أجريت الدراسه على وسط مسامى ذى حبيبات دائريه بأقطار 3, 5 ,8 mm و $0.05 \le D \le 0.125$ ، $0.1 \le R_i \le 0.9$ وكذلك لاتحدار فى الضغط B يصل الى 10^8 وأظهرت التأثيرات اللادارسيه تأثيرا كبيرا على شكل توزيع السرعه فى مقطع المجرى الحلقى، وقد ظهرت هذه التأثيرات بشكل واضح فى المناطق الملاصقه للحوائط وأعطتها زياده كبيره فى قيمه السرعه مما عمق من اندفاع سريان المائع فى هذه المناطق وأعطى بالتبعيه تأثيرا كبيرا على سلوك توزيع درجات الحراره فى المجرى وعلى طول المدخل الحرارى وكذلك على معدلات انتقال الحراره معلقه فى عدد نوسيلت على حوائط المجرى. وقد أعطت النتائج معلومات كامله ومفيده عن شكل السريان وانتقال الحراره فى مدى المتغيرات المذكوره وكذلك تم الحصول على علاقات مفيده تصيغ إعتماد طول المدخل الحرارى على المتغيرات المختلفه (d, D, B, R_i).

Abstract:

Forced convection heat transfer and flow in an annular channel filled with saturated porous media has been numerically studied. The temperature at the channel walls was asumed constant. Besides the energy equation, the generalized form of the momentum equation including the non-Darcian effects such as the variable porosity, flow inertia, and viscous friction is considered, and the finite difference method is used. To verify the numerical results a comparison has been done with the results obtained by Poulikakos and Renken [6]. The comparison shows a very good agreement for the presented results and proves the validity of the model. The results have been obtained numerically for sphere beads (3, 5 and 8 mm diameter), $0.05 \le D \le 0.125$, $0.1 \le R_i \le 0.9$ and nondimensional pressure gradient B up to

Recieved on 21-7-1994

10^8. The non-Darcian effects have a significant influence on the velocity profiles. These effects appear clearly in the regions near the walls and gives an increase in the magnitude of the velocity and signifies the channeling effect. It has in turns a significant influence on the behavior of the temperature, thermal entry length and Nusselt number across and at the channel walls. The results give complete information about the flow structure and heat transfer for the expressed ranges of parameters. Also, useful correlations reporting the dependence of the thermal entry length on the problem parameters (d, D, D and R_i) were reported.

1. Introduction

Heat transfer in porous media has been the subject of numerous investigations due to increasing interest in chemical catalytic reactors, building thermal insulation, heat exchangers, petroleum reservoirs, geothermal operations, packed-sphere beds, and many others. This increased use of porous media has made it essential to have a better understanding of the associated transport processes. First to improve the performance of existing porous-media-related thermal systems, and second to generate new ideas and explore new avenues with respect to the use of porous media in heat transfer applications.

The transport of momentum and thermal energy in fluid saturated porous media with low porosities is commonly described by Darcy's model. The main limitations of the Darcy flow model are that it is not appropriate for fast flows, it does not satisfy the no-slip condition on a solid boundary and does not account for the spatial variation of the matrix porosity. Certain porous materials such as foam, metals and fibrous media, usually have high porosity. In these media the boundary and inertia effects not included in the Darcy's model may alter the flow and heat transfer characteristics. To this end, the Works of Vafia and Tien [1], Vafia et al. [2], and Vafia [3] are releavant. The work of Vafia and Tien [1] constitutes one of the first theoretical attempts to account for boundary and inertia effects in porous media forced convection. To account for the effect of a solid boundary, Kaviany [4] studied the forced convection heat transfer in a porous channel bounded by isothermal parallel plates based on the Brinkman-extended Darcy model, and Nakayama et al. [5] treated the wall by a constant heat flux and peripherally uniform wall temperature. Poulikakos and Renken [6] investigated the effects of flow inertia, variable porosity, and solid boundary on forced convective flow through porous media between parallel plates or in circular pipes. They found that the boundary and inertia effects decrease the Nusselt number, whereas the effect of flow channeling increases the Nusselt number. Furthermore, Prasad et al. [7] have suggested that the effective thermal conductivity should not be the one based on stagnant fluid conditions, but should include a contribution

from convective motion. Similar concepts in forced convective heat transfer in a channel have been used by Cheng et all. [8]. The impact of flow inertia in natural convection problems has been investigated by Poulikakos [9] and Bejan and Poulikakos [10]. In addition to the above, an analysis for the importance and relevance of non-Darcian effects associated with the buoyancy driven convection in open-ended cavities filled with fluid-saturated porous medium was done by Ettefagh et al. [11]. The Variable porosity close to an impermeable boundary leads to a number of important effects such as flow maldistribution and channeling. Channeling, which refers to the occurance of a maximum velocity in a region close to an external boundary, has been reported by a number of investigators such as Benenati and Brosilow [12]. They show a distinct porosity variation in packed beds. Their results show a high porosity region close to the external boundary. Chandrasekhara and Vortmeyer [13] used the measurements of Benenati and Brosilow [12] to solve numerically for the velocity profile in isothermal packed beds.

The objective of the present work is to analyze an interesting problem which is of both fundamental and practical interest, . It relates to several of the above mentioned thermal engineering applications, namely, the problem of forced convection in an annulus channel filled with porous material. The formulation is general enough to include non-Darcy effects As applied in this work, factors leading to the breakdown of Darcian flow arise from inertial forces, viscous friction (Brinkman friction) in the liquid phase and variable porosity near the solid boundary. It is worth noting that unlike the hydrodynamic entry length, which is usually short in porous media channel flows, very little is known about the thermal entry length. One of the main goals of this study is to present detailed results on the thermal entry region by using the general flow model

2. Mathematical Formulation and numerical solution

Figure 1 shows the physical system and the coordinate employed to describe the flow field. It shows a porous layer (annulus) bounded by two concentric cylindrical walls. The porous medium is isotropic, homogeneous and saturated with an incompressible fluid. Both cylinders are kept at constant temperature T_w, and the fluid at the inlet to the annulus portion is isothermal at T_{in} with $T_{in} \neq T_w$

In this study a saturated porous medium consisting of packed spheres is used to illustrate the results. It will be treated as a continuum with solid and fluid phases in local thermodynamic equilibrium, properties of the fluid and the porous medium such as viscosity, thermal conductivity, thermal expansion coefficient and effective thermal diffusivity are constant. Under these assumptions the energy equation can be written as:

$$u\,\partial T/\partial x = \alpha_e \cdot 1/r \cdot \partial/\partial r\,(r\,\partial T/\partial r) \qquad (1)$$

In order to study transport through high porosity media, the original model of Darcy is improved by including the boundary friction (viscous term) and inertia effects. Under this condition the x-momentum equation can be written in terms of their macroscopic (physically) measurable properties of the flow as follows:

$$0 = -1/\rho\,[\partial P/\partial x] + \upsilon/r\,[\partial/\partial r\,(r\,\partial u/\partial r)] - \upsilon\,u/\gamma - A\,u^2 \qquad (2)$$

In the above equations u, P, T, ρ, α_e, υ are the velocity in the axial direction x, the pressure, the temperature, the fluid density, the effective thermal diffusivity and the fluid dynamic viscosity respectively. γ and A are the permeability and the inertia coefficient (Forschheimer function) of the porous medium and are dependent on the porosity ε and other geometrical parameters of the medium. When the porous medium is made of identical spherical beads with diameter d, the permeability and the inertia coefficient γ and A can be estimated as follows [14]:

$$\gamma = d^2\,\varepsilon^3 / [\,175\,(1-\varepsilon)^2\,] \qquad (3)$$

$$A = 1.75\,(1-\varepsilon)/[\,d\,\varepsilon^3\,] \qquad (4)$$

In equation (2) the buoyancy term has been neglected, since the present study deals with forced convection in an annulus filled with porous medium. The second term of the right hand side of equation (2) accounts for the friction due to macroscopic shear and was introduced first by Brinkman [15]. The term multiplied by A in equation (2) was first introduced by Forschheimer in an empirical manner for the special case of one dimensional flows through porous media, in order to account for inertial effects [15]. The third term is responsible for the porous structure. Note that by keeping the first and third terms on the right hand side of equation (2) and neglecting the rest of them, the momentum equation reduces to that for the familiar Darcian flow. On the other hand, when the porosity $\varepsilon = 1$ and the permeability $\gamma \to \infty$, Equation (2) reduces to the convectional momentum equation for pure fluid flow.

The functional dependence of the porosity on the distance from the boundary (wall) can be found from the experimental results of Benenati and Brosilow [9]. These results can be represented very well by an exponential function of the following form, which is used later by Vafia et.al [2], Poulikakos and Renken [6], and Mularidhar and Kulacki [16]:

$$\varepsilon = \varepsilon_e \left[1 + b \exp(-c\, y / d)\right] \qquad (5)$$

Where y is the distance from the boundary wall, ε_e is the free stream porosity, and the empirical constants b and c are dependent on the particle diameter.

Equation (5) neglects the small oscillations of the porosity which are considered to be secondary. The emphasis here is on the decay of the porosity from the external surface which has primary effect. The results will be illustrated by using spheres 3, 5 and 8 mm in diameter. These sphere sizes are commonly used in laboratory experimental bed to particle diameter ratios of 15, 10 and 6.5 respectively. The constants chosen to represent the variation of ε_e, b, and c are similar to that used by Benenati and Brosilow [9] and Chandrasekhara and Vortmeyer [10]. They are $\varepsilon_e = 0.37$ for d = 3, 5, 8 mm, b = 0.35, 0.43, 0.9 and c= 3, 3, 2 for d = 3, 5, 8 mm respectively.

The boundary conditions imposed on the physical system are uniform with respect to the axial coordinate, the computational domain thus comprises of one half of the annulus over which the following boundary conditions are applied:

$T = T_w$ and $u = 0$ at both the boundaries $r = r_i$ and $r = r_o$

$T = T_{in}$ at the inlet section where $x = x_{in}$.

It is convenient to cast the governing equations (1) and (2) in dimensionless form by introducing the new nondimensional variables

$$U = u / (\upsilon / r_o), \quad R = r/r_o, \quad X = (x - x_{in}) / (r_o \cdot Pr), \quad \theta = (T_w - T) / (T_w - T_{in})$$

The resultant nondimensional governing equations (1) and (2) are written as:

$$U\, \partial\theta / \partial X = 1/R \cdot [\partial / \partial R\, (R\, \partial\theta / \partial R)] \qquad (6)$$

$$U + C_1 U^2 = B\, C_2 + C_2 / R \cdot [\partial / \partial R\, (R\, \partial U / \partial R)] \qquad (7)$$

where $C_1 = 0.01\, D / (1 - \varepsilon)$, $\quad B = -\partial P / \partial x \cdot [r_o^3 / \rho \upsilon^2]$,

$C_2 = D^2\, \varepsilon^3 / [175 (1 - \varepsilon)^2]$

and D is the sphere diameter to the channel outer radius ($D = d / r_o$)

The effect of the fluid motion on the local heat flux at the channel walls can be expressed by the conduction referenced Nusselt number which is defined in the dimensionless form as [6]:

$$Nu_w = \partial T/\partial r \Big|_{r=r_w} \cdot [r_o/(T_w - T_m)] \qquad (8)$$

where the subscript w refers to either i or o for the inner and outer walls of the duct, T_m is the mixed mean fluid temperature defined in a manner similar to that for classical fluid duct flows:

$$T_m = \left(\int_{r_i}^{r_o} \rho u T \, dr \right) / [\rho V (r_o - r_i)]$$

where

$$V = \left(\int_{r_i}^{r_o} u \, dr \right) / (r_o - r_i)$$

Finite difference equations are derived from equations (6) and (7) by integration over finite area element, following the procedure developed by Patankar [17]. Since equation (7) pertains the forced convection, it can be solved independently to get the velocity field, and with this information in hand, the temperature field can be obtained from the energy equation (6). Both the first and second order derivatives in the momentum equation (7) were discretized by using central difference formulae [18]. The Forschheimer nonlinear term is linearized by guessing initial valued of the velocity field at all the grid points, and the nonlinear term was written as the product of the unknown velocity and the guessed velocity. The difference algebraic equations are solved using the Gauss-elimination method [17] to yield the velocity field. Once the velocity field have been determined, a numerical solution for the energy equation was carried out based on the very powerful and convenient equation solver mainly the TDMA. [18]. After the determination of the temperature field, equations (8) for both the two walls are integrated and the local Nusselt number at both the inner and outer walls of the duct can be calculated. A variable grid for accurate resolution of the important near-wall region is used in the Y-direction to obtain the momentum equation finite difference form. A very fine grid size in the X direction near the channel inlet and coarser downstream is used to capture the steep changes in the temperature field near the entrance.

3. Results and Discussion

3.1 Validation and Comparison

The program developed for this study was validated. Since there was no previous investigation of boundary and inertial effects in an annulus geometry, a comparison was done with the results obtained by Poulikakos and Renken [6] for the case of the flow in a cylindrical channel filled with porous medium, including the effects of flow inertia, variable porosity, and Brinkman friction.

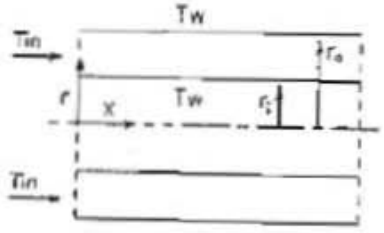

Fig. 1 Physical model, Coordinate system and thermal boundaries

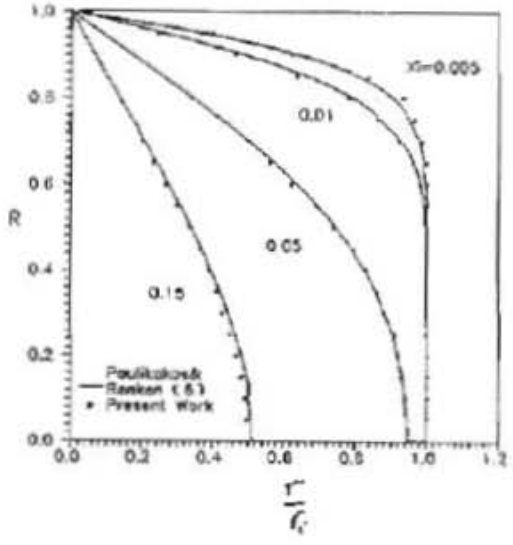

Fig. 2 Temperature distribution across the circular pipe. d = 3mm, D = 0.1, and B = 10^7

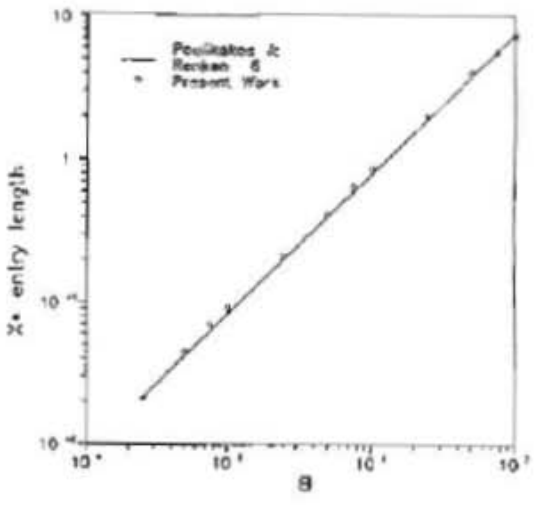

Fig. 3 Dependence of thermal entry length for the circular pipe on B. d = 3mm, D = 0.1

Figs. (2) and (3) present the temperature distribution across the channel width and dependence of the thermal entry length on the nondimensional pressure gradient parameter B for the circular pipe configuration for sphere diameter of 3mm. The comparison shows a very good agreement and proves the validity of the model.

3.2 Flow Velocity Profile

The Variable porosity close to an impermeable boundary leads to a number of important effects such as flow maldistribution and channeling. The effect of the different geometric parameters of the described model on the channeling effect and flow velocity is studied in order to give good explanations for the variation of the Nusselt number and temperature distribution across the channel and the effect of these parameters on the thermal entry region which will be obtained below.

Fig. (4) shows the velocity distribution for different values of D from 0.05 to 0.125 for sphere diameter of 3mm and $B= 10^5$. The non-Darcian effects appear clearly only in the regions near the walls, which gives an increase in the magnitude of the velocity and signifies the channeling effect. This effect increases with the increase of D (the sphere diameter / the duct outer radius), i.e. with the increase of the permeability near the walls. Fig. (5) pertains the velocity distribution across the channel half width for different values of the nondimensional pressure gradient B for d=3mm and D=0.1. Increasing the sphere diameter to the channel outer radius ratio D and increasing the nondimensional pressure gradient B, yields an overall increase in the fluid velocity, i.e. faster flow in the duct, with no other significant qualitative difference.

Fig. (6) presents the dependence of the flow velocity across the channel half width on the sphere diameter d for D= 0.1 and $B= 10^5$. With the increase of the sphere diameter the velocity near the walls increases. That is because of the increasing permeability near the walls which increases the channeling effect.

Fig. (7) shows the flow velocity distribution across the channel half width for different values of duct radius ratio R_i (the radius of the inner cylindrical wall to the radius of the annulus duct $R_i = r_i/r_o$), for sphere diameter d=3mm, D=0.1 and $B= 10^5$. The change of the inner radius of the channel R_i makes no change in the channeling effect near the duct walls, and also in the qualitative or quantitative behavior of the velocity near the duct walls, or in the core of the duct. But due to the decrease of duct thickness with the increase of R_i, the mean flow velocity increases

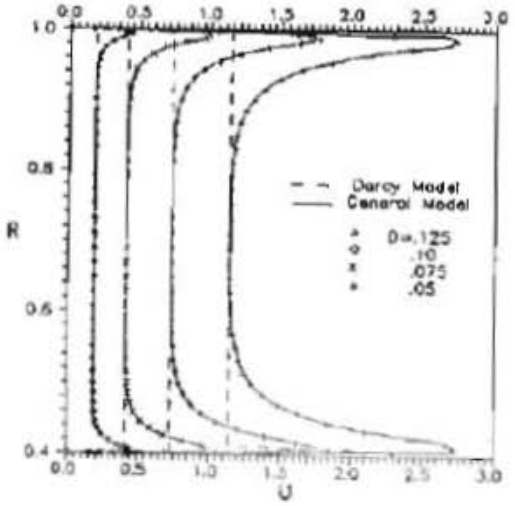

Fig. 4 Velocity distribution acroos the annulus for different values of D, d = 3mm, R_i=0.4 and B = 10^7

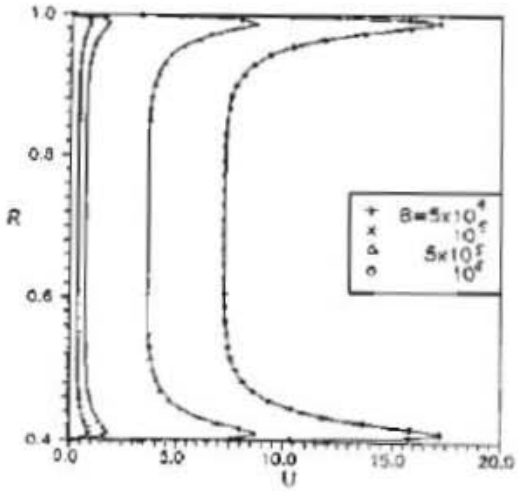

Fig. 5 Flow Velocity distribution acroos the annulus for different values of B, d = 3mm and D = 0.1

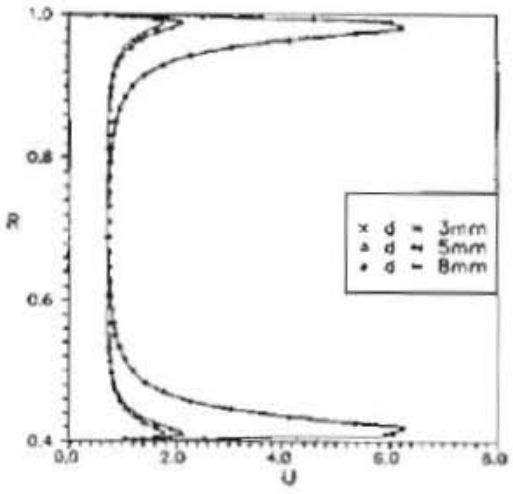

Fig. 6 Dependence of the flow velocity distribution acroos the annulus on the sphere diameter for B = 10^5, R_i=0.4 and D = 0.1

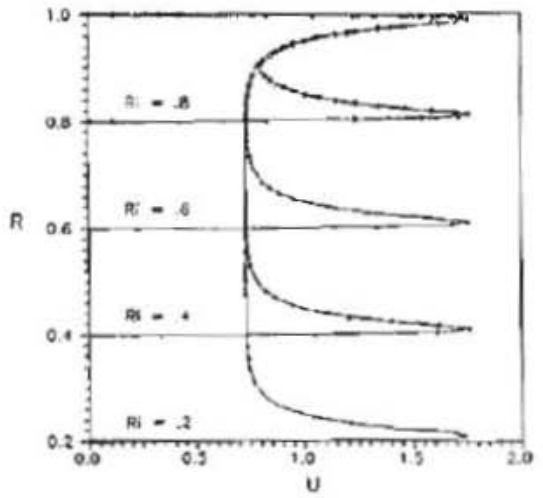

Fig. 7 Flow Velocity distribution acroos the annulus for different values of R_i, d = 3mm, D = 0.1 and B = 10^5

3.3 Thermal Entrance Length

One of the main goals of this study is to present detailed information about the thermal entry length. The thermal entrance length was defined as the distance between the entrance of the annulus duct and the point at which the Nusselt number became independent of the X location.

Fig. (8) shows the dependence of the thermal entry length X^* on the dimensionless pressure gradient B for D=0.1, R_i =0.4 and several sphere diameters, namely 3, 5 and 8 mm. A linear relation in the logarithmic graph shows that with the increasing of the nondimensional pressure gradient B and the sphere diameter d the thermal entrance length increases. Figs. (4,5) show the increasing of the flow velocity near the walls with the increase of both B and d, this makes the boundary layer thickness thinner and leads to the increase of the thermal entry length. These relations can be correlated as follows:

$$X^* = 3.5023 \times 10^{-7}\ B^{0.941} \qquad \text{for } D = 0.1,\ d = 3mm$$

$$X^* = 4.0584 \times 10^{-7}\ B^{0.9399} \qquad \text{for } D = 0.1,\ d = 5mm$$

$$X^* = 6.655 \times 10^{-7}\ B^{0.9389} \qquad \text{for } D = 0.1,\ d = 8mm$$

Fig (9) presents the dependence of the thermal entry length on D. Again, it can be seen that a linear behavior exists showing the increase of the entrance length with the increase of both D and d. This relations were correlated by the following:

$$X^* = 17.316\ D^{2.026} \qquad \text{for } B = 10^5,\ d = 3mm$$

$$X^* = 18.018\ D^{2.003} \qquad \text{for } B = 10^5,\ d = 5mm$$

$$X^* = 39.976\ D^{2.136} \qquad \text{for } B = 10^5,\ d = 8mm$$

Fig. (10) presents the behavior of the entry length with the change of duct radius ratio R_i ($R_i = r_i/r_o$) for D = 0.1, d=3mm and a host of nondimensional pressure gradient values B. The entrance length X^* decreases with the increase of R_i and increases with the increase of B. With the increase of R_i the flow velocity near the wall does not change, but the mean velocity of the flow increases. In spite of this the thermal entry length decreases due to the decrease of the thickness of the porous flow area ($r_o - r_i$). This relation can be correlated by the following:

$$X^* = [3.78 \times 10^{-7}\ B - 0.00716]\ R_i + 2.435 \times 10^{-7}\ B + 0.0072$$

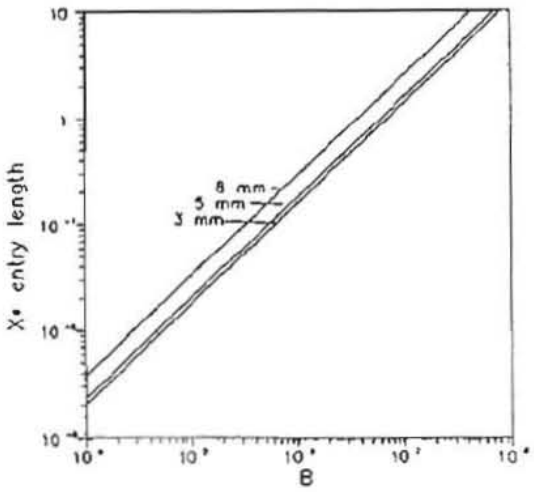

Fig. 8 Dependence of the thermal entry length on the parameter B for $R_i = 0.4$ and $D = 0.1$

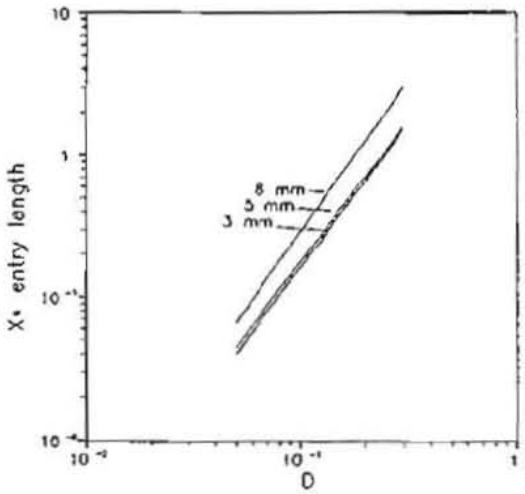

Fig. 9 Dependence of the thermal entry length on D for $R_i = 0.4$ and $B = 10^5$

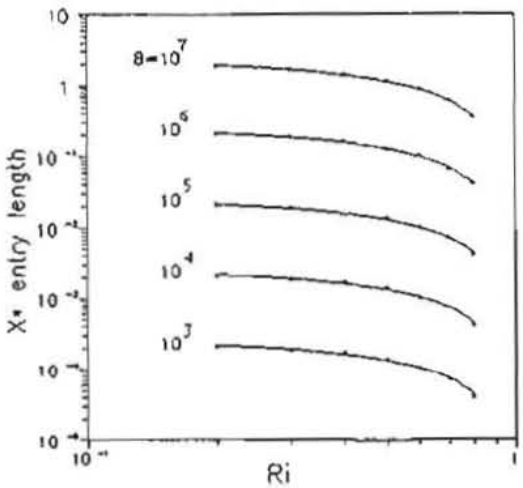

Fig.10 Behavior of the thermal entry length with the change of the duct ratio R_i for d = 3mm and $D = 0.1$

3.4 Temperature Variation

Figs (11)-(13) represent the nondimensional temperature variation across the duct half width at several downstream locations for D=0.1, sphere diameters 3 and 5 mm, and B= 10^5 and sphere diameter 3mm and B=10^6 respectively. The cooling effect of the wall propagates faster in the duct with smaller sphere diameter and for the smaller pressure gradient B. This result is correct from the physical standpoint since decreasing B and the sphere diameter d yields slower flow in the duct (Figs. 5 and 6), and thicker thermal boundary layers which requires shorter distances to develop as shown in Fig.(8).

3.5 Nusselt Number Variation

Figs (14) and (15) exemplify the variation of the Nusselt number along the thermal entry region at both the inner and outer walls of the duct for a wide range of nondimensional pressure gradient parameter B. Decreasing B (slower flow) yields smaller values of Nu throughout the thermal entry region. However, it is interesting to note that the various curves corresponding to different values of B up thermal entry region converge toward a single value in the thermally fully developed region.

Fig. (16) pertains the variation of the Nusselt number along the thermal entry region at both the inner and outer walls of the duct for sphere diameter of 3, 5 and 8 mm. Decreasing the sphere diameter leads to slower fluid flow which gives thicker thermal boundary layers which in turns requires shorter distances to develop. This gives lower values of Nusselt number at both the inner and outer duct walls.

Figs. (17) and (18) report the variation of the values of the Nusselt number in the thermal entry and the fully developed regions at both the inner and outer duct walls for a wide range of inner radius ratio R_i. Increasing the radius ratio R_i, i.e. decreasing the duct thickness leads to faster flow, which in turns yields higher values of the Nusselt number at both the inner and outer walls in the thermal entry and the fully developed regions

4. Conclusion

The forced convection flow through an annular channel filled with a fluid saturated porous material is investigated. This is accomplished by employing the generalized equation of motion in porous media, which includes the non-Darcian effects, namely, the variable porosity, flow inertia, and Brinkman viscous friction.

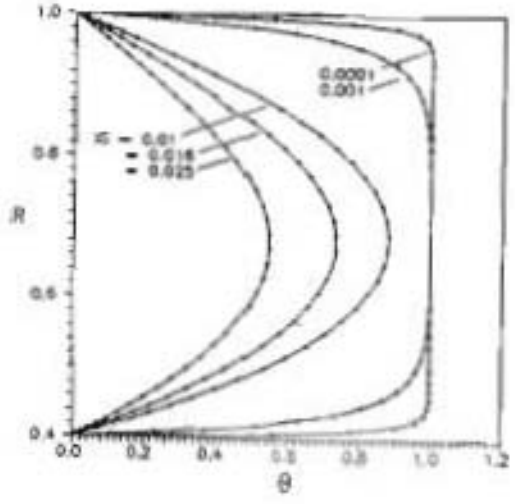

Fig 11 Dimensionless temperature distribution across the annulus pipe for $R_i = 0.4$, d = 3mm, D = 0.1 and $B = 10^5$

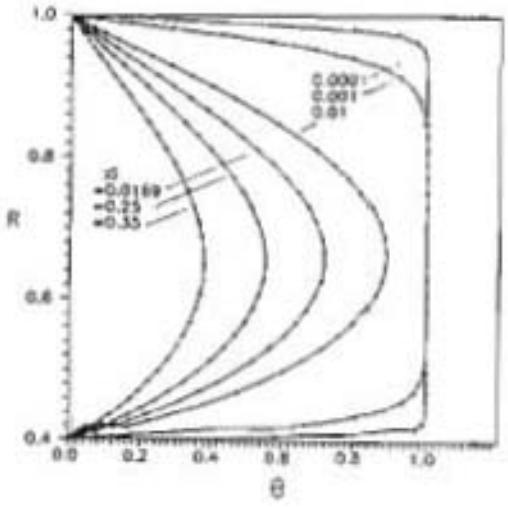

Fig 12 Dimensionless temperature distribution across the annulus pipe for $R_i = 0.4$, d = 5mm, D = 0.1 and $B = 10^5$

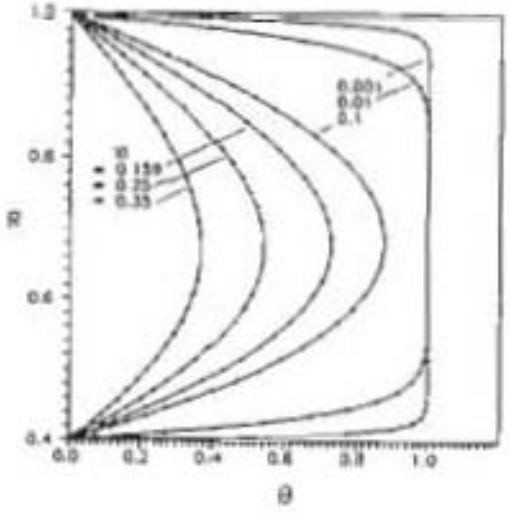

Fig 13 Dimensionless temperature distribution across the annulus pipe for $R_i = 0.4$, d = 3mm, D = 0.1 and $B = 10^6$

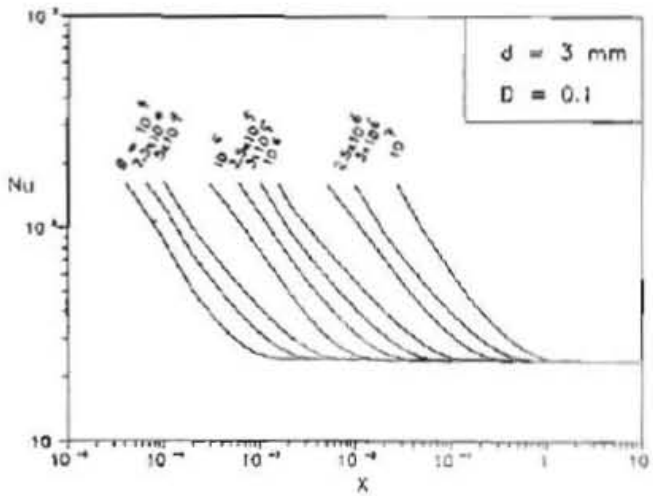

Fig. 14 Nusselt number variation with the horizontal coordinate in the thermal entry region at the inner wall of the annular pipe for a host of B values.

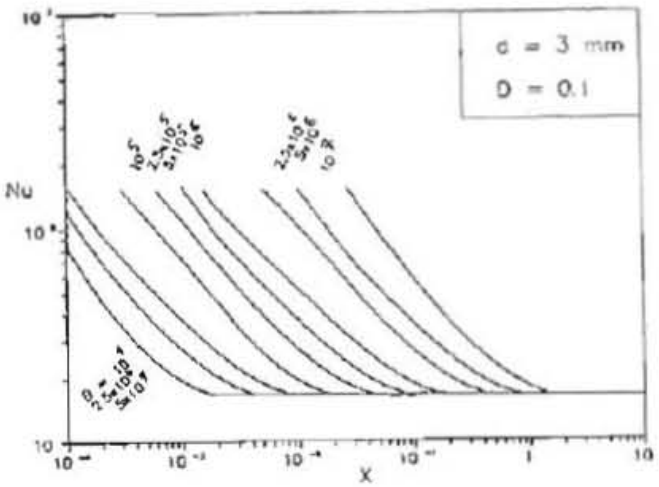

Fig. 15 Nusselt number variation with the horizontal coordinate in the thermal entry region at the outer wall of the annular pipe for a host of B values.

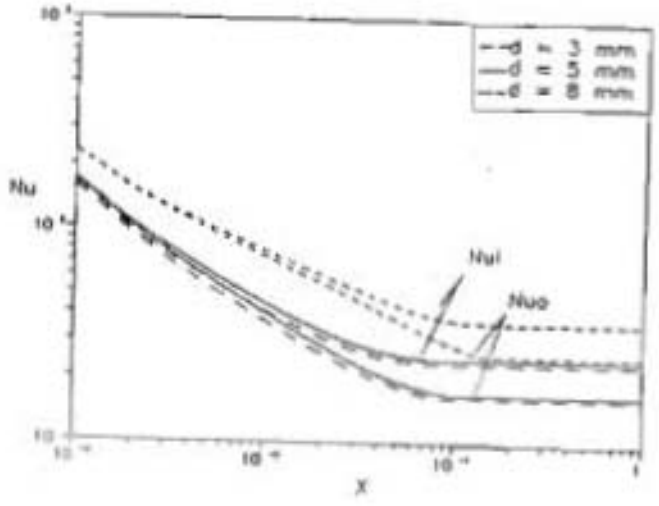

Fig. 16 Nusselt number variation in the thermal entry region at both the inner and outer duct walls for $R_i = 0.4$, $D = 0.1$ and $B = 10^5$

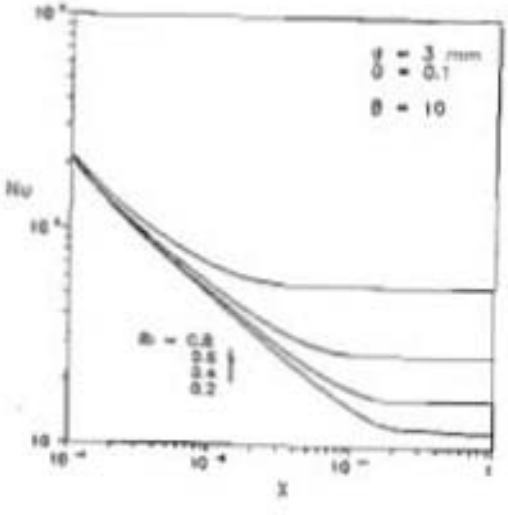

Fig 17 Nusselt number variation in the thermal entry region at the inner duct wall for d = 3mm, D = 0.1and $B = 10^5$

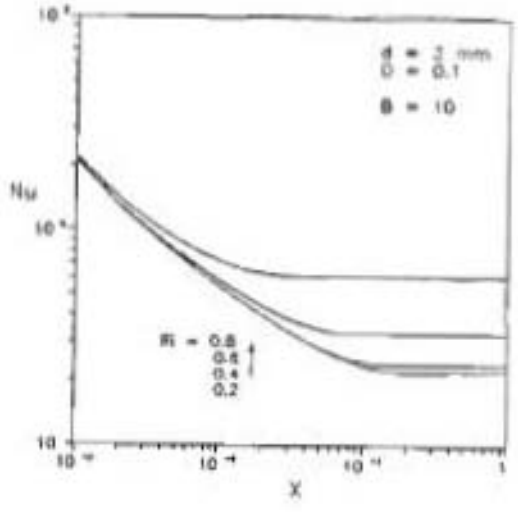

Fig. 18 Nusselt number variation in the thennal entry region at the outer duct wall for d = 3mm, D = 0.1 and $B = 10^5$

The non-Darcian effects appear clearly in the regions near the walls only, which gives an increase in the magnitude of the velocity and signifies the channeling effect. The velocity distribution across the channel including the channeling effect is the main driver for the behavior of the temperature, thermal entry length and Nusselt number across and at the channel walls.

Increasing any of the bead diameter d, the ratio of the bead diameter to the channel outer radius D, or the nondimensional pressure gradient B increases the permeability and the flow velocity in the duct and the channeling effect, which makes the boundary layer thickness thinner and leads to an increase of the thermal entry length. The cooling effects of the wall propagated slower in the duct and higher values of Nusselt number occur through out the duct inner and outer walls.

Increasing the radius ratio R_i makes no change in the channeling effects and the velocity of the flow near the walls. It increases only the mean velocity of the flow in the duct, which in turns yields faster flow and increases the Nusselt number at both the inner and outer walls in both the thermal entry region and the fully developed region. Despite of this, the thermal entry length decreases due to the decrease of the thickness of the annulus (r_o - r_i).

Useful correlations reporting the dependence of the thermal entry length on the problem parameterd (d, D, B and R_i) were also reported.

5. Nomenclature

A	Forschheimer inertia coefficient of the porous medium, equation 2
b,c	constants, equation 5
B	nondimensional pressure gradient , equation 7
C_1, C_2	dimensionless coefficients, equation 7
d	sphere diameter, mm
D	dimensionless sphere diameter = d / r_o
Nu	Nusselt number, equation 8
Nu_i, Nu_o	Nusselt number at the inner and outer walls
P	Pressure, Pa
Pr	Prandtl number = υ / α_e
r	radial coordinate
r_i, r_o	inner and outer surface radii
R	Dimensionless radial coordinate
R_i	radius ratio r_i / r_o
T	Temperature, K
T_{in}	Temperature at the inlet section x = x_{in}
T_m	average temperature, equation 8

T_w	wall temperature
u	Field velocities in the x direction, m/s
U	Non-dimensional field velocities in the X direction
x	Axial coordinate
x_{in}	channel inlet axial distance
X	dimensionless distances in the x axis
X^*	the thermal entry length
α_e	Effective thermal diffusivity of the porous medium, $m^2/$
γ	Permeability of the porous layer, equation 2, m^2
ϵ	Porosity of the porous medium
ϵ_e	free-stream porosity
θ	Non-dimensional temperature $= (T_w\text{-}T)/(T_w - T_{in})$
υ	Kinematic viscosity of the fluid, m^2/s
ρ	Fluid density , kg/m^3

6. References

1. Vafia , K., and Tien, C. L., "Boundary and Inertia Effects on Flow and Heat Transfer in Porous Media," Int. J. Heat Mass Transfer, Vol. 24, 1981, pp. 195-203.
2. Vafia, K., Alkire, R. L., and Tien, C. L., " An Experimental Investigation of Heat Transfer in Variable Porosity Media," ASME Journal of Heat Transfer, Vol. 107, 1985, pp. 642-647.
3. Vafia, K., "Convective Flow and Heat Transfer in Variable porosity Media," J. of Fluid Mechanics, Vol. 147, 1984, pp. 233-259.
4. Kaviany, M., "Laminar Flow Through a Porous Channel Bounded by Isothermal Parallel Plates," International J. of Heat and Mass Transfer, Vol. 28, 1985, pp. 851-858.
5. Nakayama, A., Koyama, H., and Kuwaha, F., "An Analysis onf Forced Convection in a Channel Filled With a Brinkman-Darcy Porous Medium; Exact and Approximation Solutions," Waerme und Stoffuebertragung, Vol. 23, 1988, pp. 291-295.
6. Poulikakos, D., and Renken, K., "Forced Convection in a Channel Filled With Porous Medium, Including the Effects of Flow Inertia, variable Porosity, and Brinkman Friction," ASME, Journal of Heat Transfer, Vol. 109, 1987, pp. 880-888.
7. Prasad, V., Kulacki, F. A., and Keyhani, M., " Natural Convection Porous Media," Journal of Fluid Mechanics, Vol. 150, 1985, pp. 89-119.
8. Cheng, P., Hsu, C. T., and Chowdhury, A., "Forced Convection in the Entrance Region of a Packed Channel With Asymmetric Heating," ASME Journal of Heat Transfer, Vol. 110, 1988, pp. 946-954.
9. Poulikakos, D., "A Departure from the Darcy Model in Boundary Layer

Natural Convection in a Vertical Porous Layer With Uniform Heat Flux from the Side," ASME Journal of Heat Transfer, Vol. 107, 1985, pp. 716-720.

10. Bejan, A., and Poulikakos, D.," The Non-Darcy Regime for Vertical Boundary Layer Natural Convection in a Porous Medium," Int. J. of Heat and mass Transfer, Vol. 27, 1984, pp. 717-722.
11. Ettefagh, J., Vafia, K., and Kim, S. J. "Non-Darcian Effects in Open-Ended Cavities Filled With a Porous Medium", ASME Journal of Heat Transfer, Vol. 113, 1991, pp. 747-756.
12. Benenati, R. F., and Brosilow, C. B., "Void fraction distribution in Packed Beds," AICHE J., Vol. 8, 1962, pp. 359-361.
13. Chandrasekhara, B. C., and Vortmeyer, D., "Flow Model for Velocity Distribution in Fixed Porous Beds Under Isothermal Conditions," Th. Fluid Dynamics, Vol. 12, 1979, pp. 105-111.
14. Rohsenow, W., and Hartnett, J. P., " Handbook of Heat Transfer", McGraw Hill, New York, 1973.
15. Cheng, P.," Heat Transfer in Geothermal Systems," Advances in Heat Transfer, Vol. 14, 1979, pp. 1-105.
16. Muralidhar, K., and Kulacki, F. A.," Non-Darcy Natural Convection in a Saturated Horizontal Porous Annulus," pp. 23-31
17. Patankar, S., "Numerical Heat Transfer and Fluid Flow" Mc Graw Hill, New York, 1980.
18. Hirsch, C., " Numerical Computation of Internal and External Flows, Vol. 1: Fundamentals of Numerical Discretization" John Wiley & Sons , 1991.